

Article

Research on Sliding Mode Control of Dual Active Bridge Converter Based on Linear Extended State Observer in Distributed Electric Propulsion System

Minsheng Yang ^{1,2,3,*}  and Pengcheng Liu ^{1,3} 

¹ College of Information and Electrical Engineering, Hunan University of Science and Technology, Xiangtan 411100, China

² College of Computer and Electrical Engineering, Hunan University of Arts and Science, Changde 415000, China

³ Key Laboratory of Hunan Province for Control Technology of Distributed Electric Propulsion Air Vehicle, Changde 415000, China

* Correspondence: yms1234@huas.edu.cn; Tel.: +86-137-8665-0414

Abstract: This paper focuses on the high-performance bidirectional DC-DC converter required in distributed electric propulsion (DEP) systems, with the dual active bridge (DAB) converter chosen as the subject of study. To achieve the goal of stabilizing the output voltage while improving the converter's anti-interference ability and dynamic performance, this paper proposes a novel strategy. In particular, it combines the Linear Extended State Observer (LESO) with a sliding mode control (SMC), proposing a sliding mode control strategy based on the Linear Extended State Observer (LESO-SMC). Notably, this control strategy not only retains the fast dynamic performance of Linear Active Disturbance Rejection Control (LADRC) and the robustness of SMC but also addresses the significant chattering issue inherent in traditional SMC. Comparing the traditional PI, LADRC, and SMC strategies, the results show that when the load changes, the voltage fluctuation of the LESO-SMC strategy proposed in this paper is 0.165 V (0.25 V) in the Matlab/Simulink and RT-Lab platforms, and the average adjustment time is 4 ms (3.5 ms). In contrast, the average voltage fluctuations of PI and LADRC strategies were 3.7 V (4.9 V) and 0.55 V (1.35 V), and the average adjustment times were 99.5 ms (201 ms) and 71.5 ms (77.5 ms), respectively. When the input voltage changes, the proposed LESO-SMC strategy adjusts faster and has almost no voltage fluctuations, while the average voltage fluctuations of the PI and LADRC strategies in the simulation are 0.5 V and 0.1 V, and the average adjustment times are 89.5 ms and 35 ms, and the change in the input voltage in the RT-Lab platform has very little effect on the output voltage. Compared with SMC, the LESO-SMC strategy has no chattering problem. In summary, compared to the other three control strategies, the LESO-SMC strategy proposed in this paper exhibits superior performance in terms of voltage fluctuation and adjustment time during load changes and input voltage changes. It shows a robust anti-interference ability and a rapid dynamic response performance.



Citation: Yang, M.; Liu, P. Research on Sliding Mode Control of Dual Active Bridge Converter Based on Linear Extended State Observer in Distributed Electric Propulsion System. *Electronics* **2023**, *12*, 3522. <https://doi.org/10.3390/electronics12163522>

Academic Editor: Adel M. Sharaf

Received: 11 July 2023

Revised: 12 August 2023

Accepted: 16 August 2023

Published: 20 August 2023



Copyright: © 2023 by the authors. Licensee MDPI, Basel, Switzerland. This article is an open access article distributed under the terms and conditions of the Creative Commons Attribution (CC BY) license (<https://creativecommons.org/licenses/by/4.0/>).

1. Introduction

With the continuous rise in global carbon dioxide emissions, countries increasingly focus on energy conservation, emission reduction, and green, sustainable development. In recent years, the new energy industry entered a phase of rapid development, with various advanced energy conversion systems being proposed. Among these, distributed electric propulsion (DEP) systems, known for their low loss and high-quality power, received special attention [1,2]. As shown in Figure 1, the DEP system obviously requires the DC-DC converter to adjust the voltage to meet different load requirements. Moreover, it also serves

as a bridge between the energy storage system and the DC bus, which can be used to balance power fluctuations [3]. Therefore, a converter with good performance is needed. Enhancing the anti-interference ability and the dynamic response speed of the DC-DC converter is also a key factor when studying the characteristics of such converters.

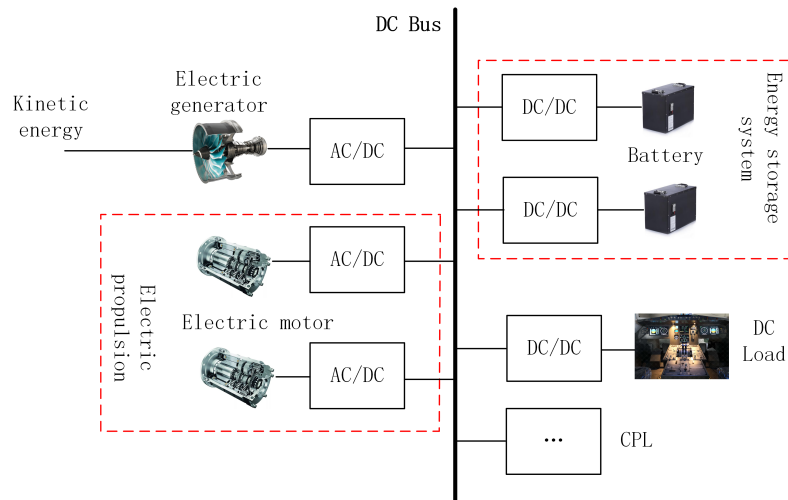


Figure 1. Distributed electric propulsion system.

The DAB converter, known for its key features such as high power transmission efficiency, electrical isolation, and bidirectional energy flow, attracts widespread attention in the new energy industry [4].

The efficiency and performance of a converter are closely related to its mathematical modeling and control strategy. Various modeling methods and control strategies are proposed by scholars to enhance the disturbance suppression ability and dynamic performance of the DAB converter. Existing research primarily includes three types of mathematical modeling: reduced-order models, generalized averaging models, and discrete-time models [5–8]. Based on these, various advanced control strategies are proposed. For example, Reference [9] borrows the idea of power control in motor control and proposes a direct power control (DPC) strategy. Building on this, reference [10] introduces a virtual power control (VPC). However, the former is easily influenced by system internal parameters, and the latter has poor robustness and dynamic performance. Reference [11] applies load current feedforward to improve the converter's dynamic performance to load changes and reduce the use of sensors, but it does not deeply analyze its stability, and its performance is poor when the parameters are inaccurate. References [12–14] apply the model predictive control (MPC) to the converter, but MPC requires strong computing power, which might lead to an increase in hardware costs, and the derivation process of the control method is complex. To address the instability problem caused by constant power loads, References [15,16] introduce Linear Active Disturbance Rejection Control (LADRC) into the converter, achieving fast dynamic performance while maintaining system stability. Sliding mode control (SMC) has strong robustness against system parameter changes and disturbances and has been validated in many industrial fields. References [17,18] employ SMC to control DAB converters, but traditional SMC suffers from the problem of chattering, which can cause serious issues during converter control.

Observer control technology is widely studied over the past few decades due to its ability to estimate and compensate for disturbances [19]. Reference [20], based on load current feedforward and combined with the Nonlinear Disturbance Observer (NOD), proposes a control strategy without a current sensor. By using NOD to estimate the load current, it regulates the bus voltage without the use of current sensors. Reference [21] combines the backstepping control with the NOD to achieve accurate voltage tracking under large signal disturbances. Reference [22] proposes a robust voltage control strategy based on the Uncertainty and Disturbance Estimator (UDE) to deal with internal and external

disturbances and uncertainties, thereby enhancing the stability of the converter system. In summary, observer technology can effectively enhance the disturbance suppression ability and improve the dynamic performance of converters. However, the observer control strategies proposed in the above articles are overly complex and not easily understandable or transferable.

Compared with the discrete model and the generalized average model, the reduced-order model of the DAB converter has excellent small signal accuracy while maintaining low complexity [23]. Therefore, this paper chooses the reduced-order model, combines the Linear Extended State Observer (LESO) in LADRC with SMC, and proposes a sliding mode control strategy based on the Linear Extended State Observer (LESO-SMC). Through the LESO, the system's internal and external disturbances and model parameter uncertainties are treated as total disturbances, and the LESO is used for precise estimation and compensation of these total disturbances. To further improve the control effect and achieve an accurate tracking of the reference output voltage, an equivalent control law is derived by constructing an error integral sliding surface in combination with SMC. Then, an improved exponential reaching law is chosen as the switching control term to ensure the global asymptotic stability of the system, and finally, an error feedback law is designed using the two observer output values. Comparative experiment results show that the LESO-SMC strategy proposed in this paper is simple and can significantly improve the anti-interference ability and dynamic performance of the DAB converter.

The organization of this paper is as follows: Section 2 introduces and analyzes the working principle of the DAB converter and carries out average dynamic modeling. Section 3 outlines the design of the converter's controller, where Section 3.1 describes the design of the LADRC strategy, Section 3.2 combines the core LESO of LADRC with SMC, proposing the control strategy suggested in this paper. Section 4 is the simulation experiments and comparative analysis of various control strategy. Section 5 presents the overall conclusion of this paper.

2. Analysis of the Working Principle of DAB Converter

The circuit structure of the DAB converter is shown in Figure 2. H1 and H2 represent the symmetrical switching bridges on the primary and secondary sides of the transformer T , respectively, which include a total of eight switching tubes, ($S_1 - S_8$). U_i and U_o , respectively, represent the input and output voltages, C_1 and C_2 are support capacitors, and L represents the equivalent inductance of the leakage inductance of the transformer and the sum of the auxiliary inductances for power transmission. U_{ab} and U_{cd} each represent the square wave voltage on the primary and secondary sides, respectively.

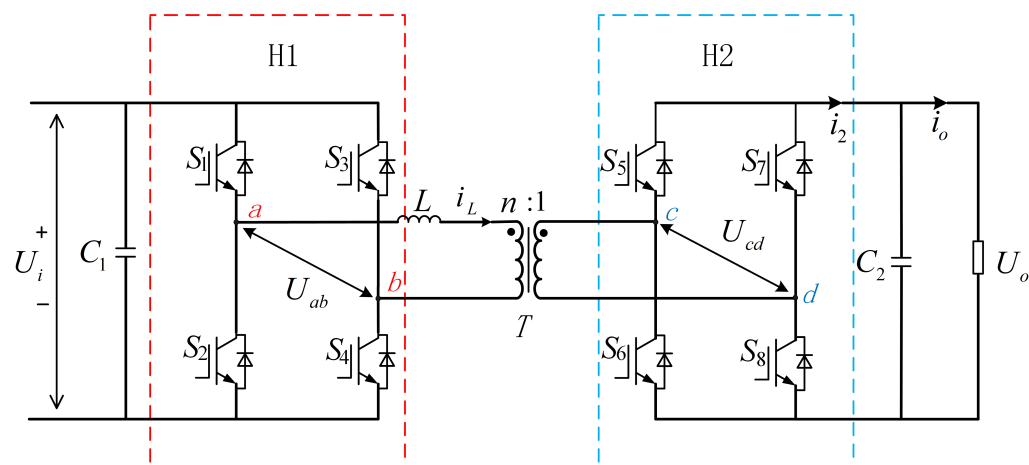


Figure 2. DAB converter circuit structure.

In order to control the DAB converter simply and effectively, the control method adopted in this paper is a single-phase-shift (SPS) control. It controls the phase shift

between the H1 and H2 bridges, denoted as D , which represents the phase difference between the square wave voltages U_{ab} and U_{cd} . D is defined as the ratio of the phase shift angle to 180° . When $D > 0$, the power is output forward (U_{ab} 's phase is ahead of U_{cd}), and when $D < 0$, the power is transmitted in reverse. To facilitate the analysis, only the case of forward power transmission is considered, and the main waveform diagram of the DAB converter under its control is shown in Figure 3. The rules for turning on and off the eight switching tubes under SPS control are as follows: within one switch period T_s ($t_0 - t_4$), the drive signals of the diagonal switching tubes in the bridges H1 and H2 are the same, and the upper and lower switching tubes in the same bridge arm are complementary. There is a certain phase difference between switching tube S_1 (S_4) of the H1 bridge and switching tube S_5 (S_8) of the H2 bridge (the phase difference between U_{ab} and U_{cd}), and all drive signals have a duty cycle of 50%.

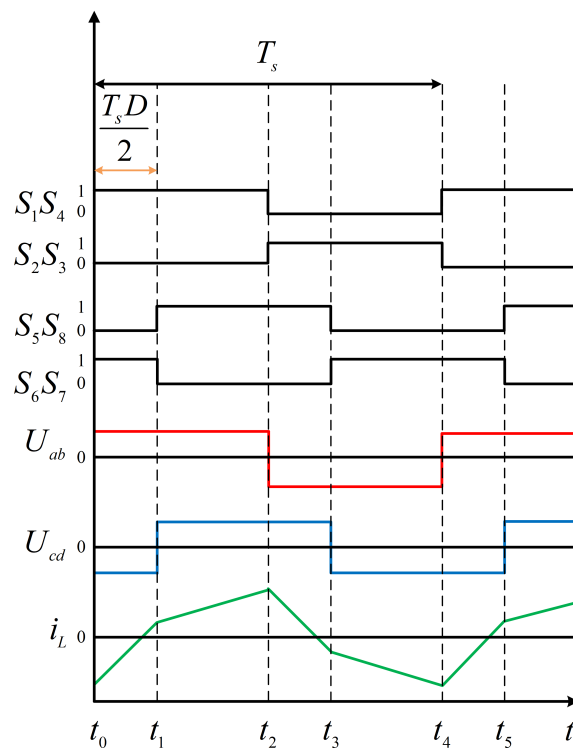


Figure 3. Single-phase-shift control waveform diagram.

As shown in Figure 3, the switching function of the DAB converter under SPS control can be defined as follows:

$$\begin{cases} S_a = \begin{cases} 1, S_1 \text{ and } S_4 \text{ ON, } S_2 \text{ and } S_3 \text{ OFF} \\ -1, S_1 \text{ and } S_4 \text{ OFF, } S_2 \text{ and } S_3 \text{ ON} \end{cases} \\ S_b = \begin{cases} 1, S_5 \text{ and } S_8 \text{ ON, } S_6 \text{ and } S_7 \text{ OFF} \\ -1, S_5 \text{ and } S_8 \text{ OFF, } S_6 \text{ and } S_7 \text{ ON} \end{cases} \end{cases} \quad (1)$$

Then, the state equation of the DAB converter can be expressed as follows:

$$\begin{cases} \frac{di_L}{dt} = \frac{S_a U_i}{L} - \frac{n S_b U_o}{L} \\ \frac{dU_o}{dt} = \frac{n S_b i_L}{C_2} - \frac{U_o}{R C_2} \end{cases} \quad (2)$$

The waveform of inductive current i_L splits into four operational phases: $t_0 - t_1$, $t_1 - t_2$, $t_2 - t_3$, and $t_3 - t_4$. By leveraging the waveform's symmetry for analytical simplicity, a half

cycle from t_0 to t_2 is selected. According to Formulas (1) and (2), the expressions for inductive current during the periods $t_0 - t_1$ and $t_1 - t_2$ are as follows:

$$i_L(t) = \begin{cases} i_L(t_0) + \frac{U_{in}+nU_o}{L}(t-t_0)t_0 \leq t \leq t_1 \\ i_L(t_1) + \frac{U_{in}-nU_o}{L}(t-t_1)t_1 \leq t \leq t_2 \end{cases} \quad (3)$$

In the Formula (3), $i_L(t_0)$ and $i_L(t_1)$ represent the inductor currents at the respective moments t_0 and t_1 , and due to the symmetry of the waveform of the inductance current i_L , it follows that $i_L(t_0) = -i_L(t_2)$, $i_L(t_1) = -i_L(t_3)$.

Neglecting system losses and combining Formula (3) and Figure 3, the power transmission P_o of the DAB converter under SPS control is defined as follows:

$$P_o = \frac{T_s}{2} \int_{t_0}^{t_2} U_i i_L(t) dt = \frac{nU_o U_i}{2L f_s} D(1-D) \quad (4)$$

f_s in the Formula (4) is the switching frequency, and $T_s = 1/f_s$.

Based on Formula (4), the average output current on the secondary side can be calculated, and a low-frequency small signal disturbance is further introduced. By eliminating the direct current and disturbances of the secondary and higher small signals, the small signal value of the output current on the secondary side can be obtained as follows:

$$\hat{i}_2 = \frac{nU_i}{2f_s L} (1-2D)\hat{d} \quad (5)$$

In Formula (5), \hat{d} is the small signal value of the shift phase ratio D , and only the output side is concerned. At this time, the corresponding small signal model of the DAB converter is shown in Figure 4:

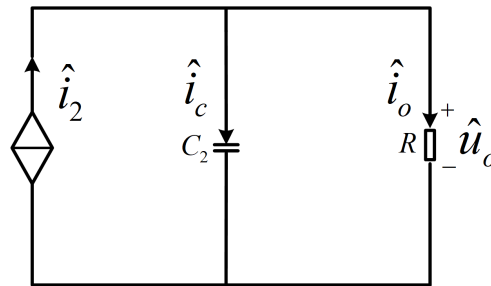


Figure 4. Small signal model of DAB converter.

From Figure 4 and Formula (5), according to Kirchhoff's current law, the dynamic equation of the output voltage can be obtained as follows:

$$\frac{d\hat{U}_o}{dt} = \frac{nU_i}{2LC_2 f_s} (1-2D)\hat{d} - \frac{\hat{U}_o}{RC_2} \quad (6)$$

In Formula (6), \hat{U}_o represents the small signal value of the output voltage U_o . Formula (6) can be further simplified as follows:

$$\dot{y} = b_0 u + f \quad (7)$$

In Formula (7), f represents the total disturbance, which includes both the unknown disturbances from the system and external sources as well as the uncertain parameters of the converter. b_0 represents the known part of the input control gain.

3. Controller Design of DAB Converter

The working performance of the DAB converter is closely related to its control strategy. The traditional PI control of the DAB converter has problems such as weak anti-interference ability and slow response speed. Therefore, this chapter combines LESO with SMC, significantly improving the anti-interference ability and dynamic response speed of the converter.

3.1. Design of Linear Active Disturbance Rejection Control

LADRC is a control strategy with good dynamic performance and certain anti-interference ability. Applying the LADRC to the DAB converter can improve its dynamic performance and anti-interference ability. The framework of the LADRC strategy is shown in Figure 5. Its LESO is the core part of LADRC. It is a dynamic observer. Its main function is to estimate the system state variables. It can extend the disturbances inside and outside the system into new state variables and compensate them to the control signal. Through the LESO, the overall dynamic performance and stability of the system can be improved [24].

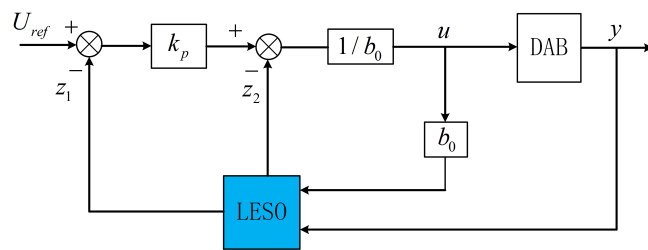


Figure 5. LADRC strategy framework.

The selection of state variables is given as $x = [x_1 \ x_2]^T = [y \ f]^T$, turning Formula (7) into a state-space equation description [25] as follows:

$$\begin{cases} y = x_1 \\ \dot{x}_1 = b_0 u + x_2 \\ \dot{x}_2 = f \end{cases} \quad (8)$$

In Formula (8), y denotes the system's output (output voltage U_o), u stands for the system's control variable (shift phase ratio D), and x_2 signifies the total disturbance extended into a state variable. Building on Formula (8), the following depicts the matrix equation for constructing the LESO as follows:

$$\begin{bmatrix} \dot{z}_1 \\ \dot{z}_2 \end{bmatrix} = \begin{bmatrix} -\beta_1 & 1 \\ -\beta_2 & 0 \end{bmatrix} \begin{bmatrix} z_1 \\ z_2 \end{bmatrix} + \begin{bmatrix} b_0 & \beta_1 \\ 0 & \beta_2 \end{bmatrix} \begin{bmatrix} u \\ y \end{bmatrix} \quad (9)$$

In Formula (9), z_1 and z_2 are the observed values of state variables y and f , respectively. β_1 and β_2 are the gain parameters of the observer. Adjusting these two gain parameters can enable the observer to estimate state variables well. To simplify the selection of parameters, the gain parameters can be chosen using the bandwidth method [26] as follows:

$$\begin{cases} \beta_1 = 2\omega_0 \\ \beta_2 = \omega_0^2 \end{cases} \quad (10)$$

According to the Hurwitz stability criterion, the selection of parameters should satisfy the characteristic polynomial equation $s^2 + \beta_1 s + \beta_2 = (s + \omega_0)^2$ to ensure the convergence of the LESO.

For the LESO, the input signals are output voltage U_o and shift phase ratio D , while the output signals z_1 is the estimated value of the output voltage U_o , and z_2 is the esti-

mated value of the total disturbance f . By substituting Formula (10) into Formula (9) and performing Laplace transform, we have the transfer function G_1 as follows:

$$G_1 = \frac{z_2(s)}{U_o(s)} = \frac{\omega_0^2 s}{s^2 + 2\omega_0 s + \omega_0^2} \quad (11)$$

Furthermore, the transfer function G_2 between the disturbance observation z_2 and the total disturbance f can be derived as follows:

$$G_2 = \frac{z_2(s)}{f(s)} = \frac{\omega_0^2}{s^2 + 2\omega_0 s + \omega_0^2} \quad (12)$$

The Bode plots of the transfer functions in LESO under different bandwidths ω_0 are shown in Figure 6. The tracking performance of LESO is better when the bandwidth ω_0 is larger. However, as ω_0 increases, the noise immunity of LESO weakens, creating an inevitable trade-off between noise immunity and disturbance rejection capabilities. Therefore, when choosing ω_0 , a balance should be struck between noise immunity and disturbance rejection capabilities. After consideration, $\omega_0 = 1600$ rad/s is chosen in this paper.

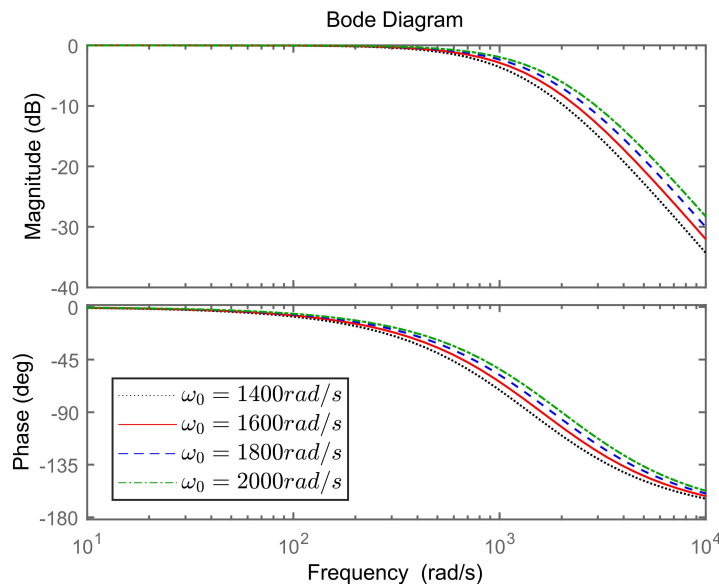


Figure 6. Bode diagram.

When the gain parameters for LESO are appropriately chosen, z_1 tends to the output voltage U_o and z_2 tends to total disturbance f . After compensation, the system is simplified to a single integral series system. Good control results can be achieved with just a linear K_p proportional control, enhancing the system's dynamic response performance.

In this case, the control signal u can be expressed as follows:

$$u = \frac{k_p(U_{ref} - U_o) - f}{b_0} \quad (13)$$

In Formula (13), $k_p(U_{ref} - U_o)/b_0$ represents the feedback control component, and $-f/b_0$ represents the disturbance compensation component.

3.2. Design of Sliding Mode Control Based on Linear Extended State Observer

While the aforementioned LADRC strategy improves the dynamic performance and anti-interference ability of the converter, considering the non-linear characteristics of the DAB converter, the linear feedback control law might not be suitable. The introduction of

SMC into the LADRC structure and the design of non-linear state error feedback law can further improve the converter's ability to suppress disturbances. However, in traditional SMC, there exists a sign function $\text{sgn}(s)$. When the system trajectory reaches the sliding mode surface, the $\text{sgn}(s)$ function causes the input control law to switch at high frequencies continuously. The inertia of the movement makes it difficult for the system state to slide along the sliding mode surface towards the desired equilibrium point, resulting in the state trajectory crossing back and forth on both sides of the sliding mode surface, thereby causing chattering. By combining SMC with the LESO from the LADRC, the LESO estimates and compensates for the total disturbance in a feedforward manner. The SMC feedback control law is designed using the observation values z_1 and z_2 and continuous functions. This reduces the switching gain in SMC, which can effectively reduce the chattering problem while improving the system response speed.

Compared with the non-integral SM control, the integral SM control can eliminate the steady-state error more effectively [27]. Therefore, in order to stabilize the output voltage while reducing the steady-state error, the constructed integral sliding surface s is expressed as follows:

$$s = k_1 e + k_2 \int e dt \quad (14)$$

In the Formula (14), k_1 and k_2 are adjustable parameters, both greater than 0, $e = U_{ref} - U_o$ is the tracking error of the output voltage, where U_{ref} is the reference value of the voltage.

Differentiating the sliding surface s and combining it with Formula (7), the formula can be obtained:

$$\dot{s} = k_1 \dot{e} + k_2 e = -k_1(b_0 u + f) + k_2 e \quad (15)$$

According to the equivalent control approach, the control law of the system can be designed as $u = u_{eq} + u_{sw}$, where u_{eq} represents the equivalent control signal, and u_{sw} represents the switching control term. Setting Formula (15) equal to 0, the equivalent control law u_{eq} can be solved as follows:

$$u_{eq} = -\frac{1}{b_0} \left(f - \frac{k_2}{k_1} e \right) \quad (16)$$

To ensure that the system reaches its equilibrium point within a finite time, the exponential convergence law can be chosen as the switching control term u_{sw} . Based on Formula (16), the final system control law u can be designed as follows:

$$u = -\frac{1}{b_0} \left(f - \frac{k_2}{k_1} e + k_3 s + \varepsilon \text{sgn}(s) \right) \quad (17)$$

The Lyapunov function can be used to analyze whether a system is stable. For the system to reach a stable state, the Lyapunov function must always be greater than zero throughout the system's entire state space, and its derivative must be less than zero. Therefore, the chosen Lyapunov function is expressed as follows:

$$V = \frac{1}{2} s^2 \quad (18)$$

To differentiate Formula (18) and substitute Formula (15) into it, the result can be obtained as follows:

$$\dot{V} = s \dot{s} = s(k_1 \dot{e} + k_2 e) = s(-k_1(b_0 u + f) + k_2 e) \quad (19)$$

Substituting Formula (17) into Formula (19), the result can be obtained as follows:

$$\dot{V} = s(-k_1(-k_3 s - \varepsilon \text{sgn}(s))) = k_1 k_3 s^2 + k_1 \varepsilon |s| \quad (20)$$

It is known that the known coefficient k_1 is greater than 0 from Formulas (18) and (20). When the selected adjustable coefficients k_3 and ε are both less than 0 and $s \neq 0$, there exists $V > 0$ and $\dot{V} = ss < 0$, satisfying the basis for Lyapunov stability judgment. In SM control, it manifests as the initial state outside the sliding mode surface $s = 0$, which satisfies the condition to reach the sliding mode surface, i.e., any initial state where $s \neq 0$ can tend toward the equilibrium point in finite time, thereby achieving a stable state for the system.

As shown in Formula (17), the control law u (the phase shift ratio D) of the system contains a high-frequency sign function $\text{sgn}(s)$. Its presence can cause the high-frequency switching of the phase shift ratio D , resulting in vibrations. For the DAB converter, the high-frequency chattering of the phase shift ratio D can cause huge fluctuations in power transmission. In addition, it may lead to an increase in the transformer current, causing core saturation, thereby increasing energy consumption and affecting the dynamic performance of the converter [28]. In order to reduce the vibration of the transient switching of the phase shift ratio D , the observed values z_1, z_2 and the continuous function $\text{sat}(s)$ are used to optimize the sign function to smooth the change in the control law. In Figure 7, (a) and (b) are comparisons of the phase shift ratio D before and after the replacement of the continuous function, and it is clear that the control law after the replacement with the continuous function is smoother.

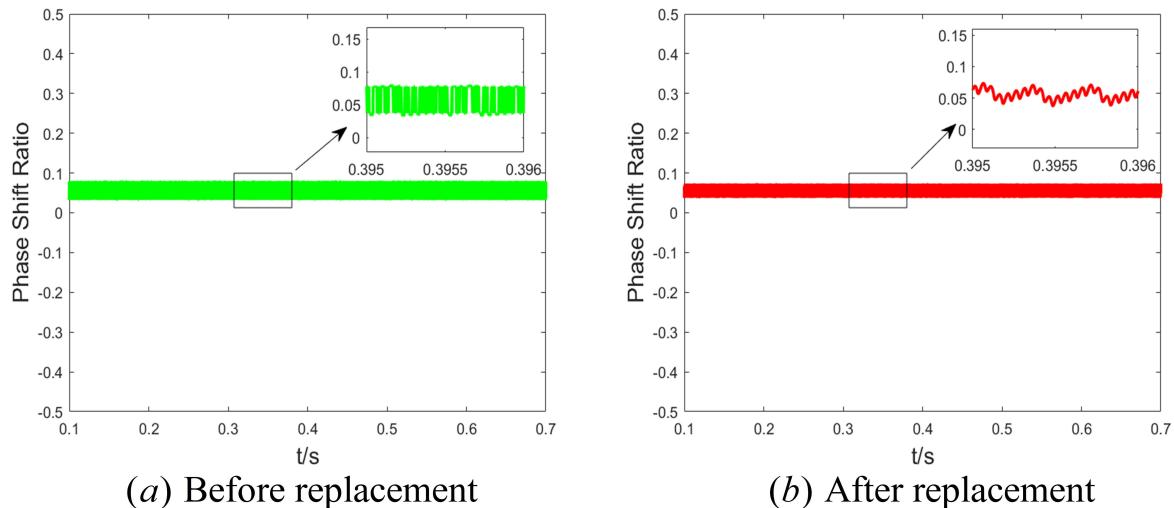


Figure 7. Comparison of phase shifts before and after continuous function optimization: (a) before replacement and (b) after replacement.

The chosen continuous function is expressed as follows:

$$\text{sat}(s) = \frac{s}{|s| + \eta} \quad (21)$$

In Equation (21), the term η is the anti-chattering factor, and $\eta > 0$.

Combining Equations (9), (17), and (21), the SMC law based on the LESO and designed using the observed values z_1 and z_2 can be expressed as follows:

$$u = -\frac{1}{b_0} (z_2 - \frac{k_2}{k_1} \hat{e} + k_3 \hat{s} + \varepsilon \text{sat}(\hat{s})) \quad (22)$$

In Equation (22), $\hat{e} = U_{ref} - z_1$, $\hat{s} = k_1 \hat{e} + k_2 \int \hat{e} dt$.

The design of LESO-SMC strategy is depicted in Figure 8, as mentioned in this article.

After collecting U_o and D to LESO, LESO outputs the estimated value z_1 of U_o and the estimated value z_2 of total disturbance. Using the errors between U_{ref} and z_1 and z_2 , the phase shift ratio D is output using Formula (22), and finally, eight switches are driven

to work. It should be noted that D generally ranges from -0.5 to $+0.5$, so the saturation module should be added in front of the output control signal.

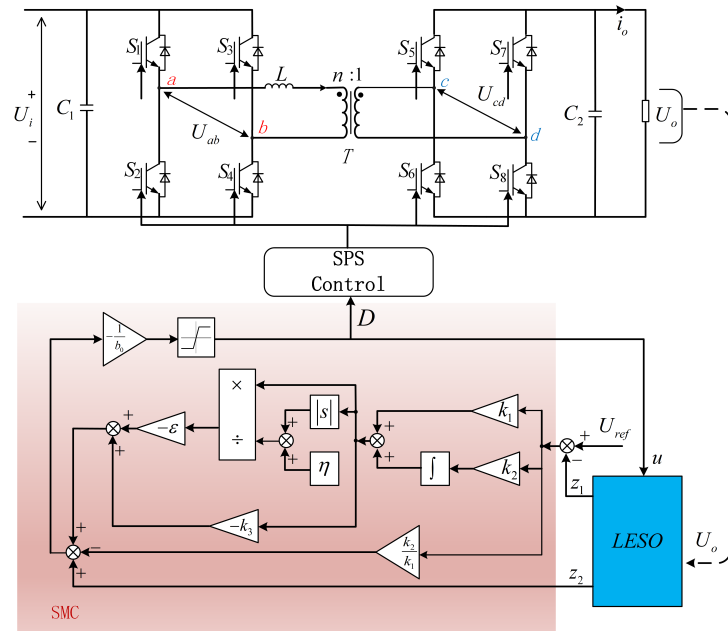


Figure 8. Block diagram of the LESO-SMC strategy.

4. Analysis of Simulation Experiment Results

To validate the superiority and feasibility of the proposed LESO-SMC strategy, a simulation model of the DAB converter is constructed using the Matlab/Simulink platform, as shown in Figure 9. The main circuit parameters are shown in Table 1.

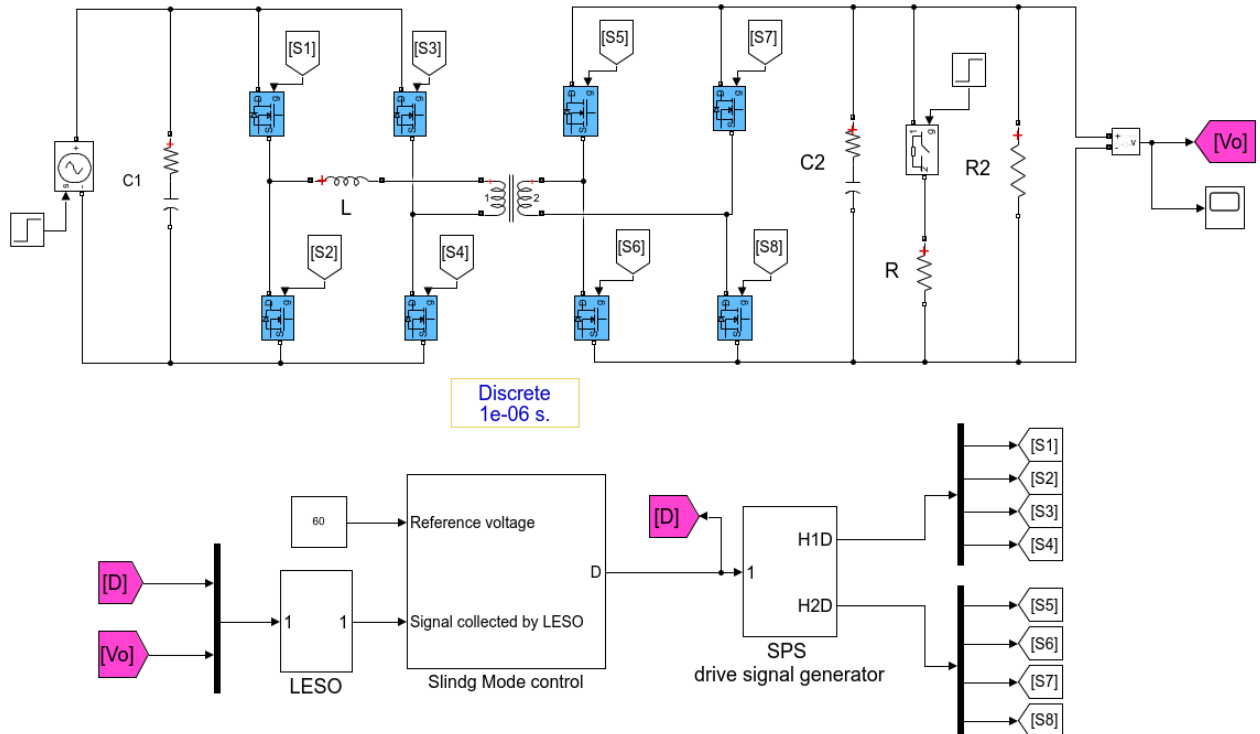


Figure 9. Simulation model of DAB converter.

Table 1. DAB converter circuit parameters.

Main Circuit Parameters	Value
Input voltage U_i /V	100
Output voltage U_o /V	60
Transformer ratio n	1:1
switching frequency f_s /Khz	10
Equivalent inductance $L/\mu\text{H}$	200
Input side capacitance $C_1/\mu\text{F}$	2000
output side capacitance $C_2/\mu\text{F}$	2000
load resistance R/Ω	30/15

This paper compares the dynamic performance and disturbance resistance of the converter's output voltage under load change and input voltage change, using four different control strategies: traditional single closed-loop voltage PI control; the LADRC; the SMC presented in reference [29]; and the LESO-SMC strategy. The parameter selection for the four control strategies are shown in Table 2.

Table 2. The parameter values of the proposed control method.

Control Methods	Parameters	Value
PI	k_p	0.05
	k_i	1.5
LADRC	b_0	2000
	ω_0	1600
	k_p	50
SMC	k_1	1000
	k_2	10
	k_3	40
	ε	40
LESO-SMC	k_1	1000
	k_2	10
	b_0	2000
	ω_0	1600
	k_3	40
	ε	40

4.1. Load Change Experiment

Figure 10 presents the output voltage dynamic performance waveform under the four control strategies during the load change. Figure 10 contains four subfigures, where (a) represents PI control, (b) shows LADRC, (c) denotes SMC, and (d) illustrates the LESO-SMC strategy proposed in this paper. The system experiences output voltage fluctuations due to the sudden load change and, after an adjustment period, recovers to the reference voltage. From the four subfigures in Figure 10, it can be noted that, when the load abruptly changes from 30Ω to 15Ω at 0.3 s, the output voltage of the PI control drops the most, about 2.9 V, and has the longest adjustment time, approximately 104 ms. The LADRC strategy experiences a smaller voltage drop of about 1.1 V, but the adjustment time is still relatively long, requiring about 78 ms. Traditional SMC strategy can rapidly regain stability after the load change with virtually no dynamic process and voltage fluctuation, but, as shown in Figure 10c, there is also notable chattering in the SMC. Additionally, the back-and-forth crossing of the control law over the sliding surface results in pronounced voltage ripples. The LESO-SMC strategy proposed in this paper requires a shorter adjustment time, recovering in approximately 3 ms, with the voltage dropping only about 0.13 V. More importantly, it resolves the issue of excessive chattering.

At 0.5 s, when the load changes from 15Ω back to 30Ω , under traditional PI control, the adjustment time is the longest, requiring 95 ms, and the output voltage increase is the largest, about 4.5 V. The LADRC strategy experiences a voltage rise of about 0.6 V, with a longer adjustment time still needed, around 65 ms. Traditional SMC strategy can quickly transition back to the original output voltage without a noticeable voltage increase, but it still presents a significant chattering phenomenon. The LESO-SMC strategy proposed in this paper requires a shorter adjustment time, needing only about 5 ms, and a smaller voltage increase of approximately 0.3 V.

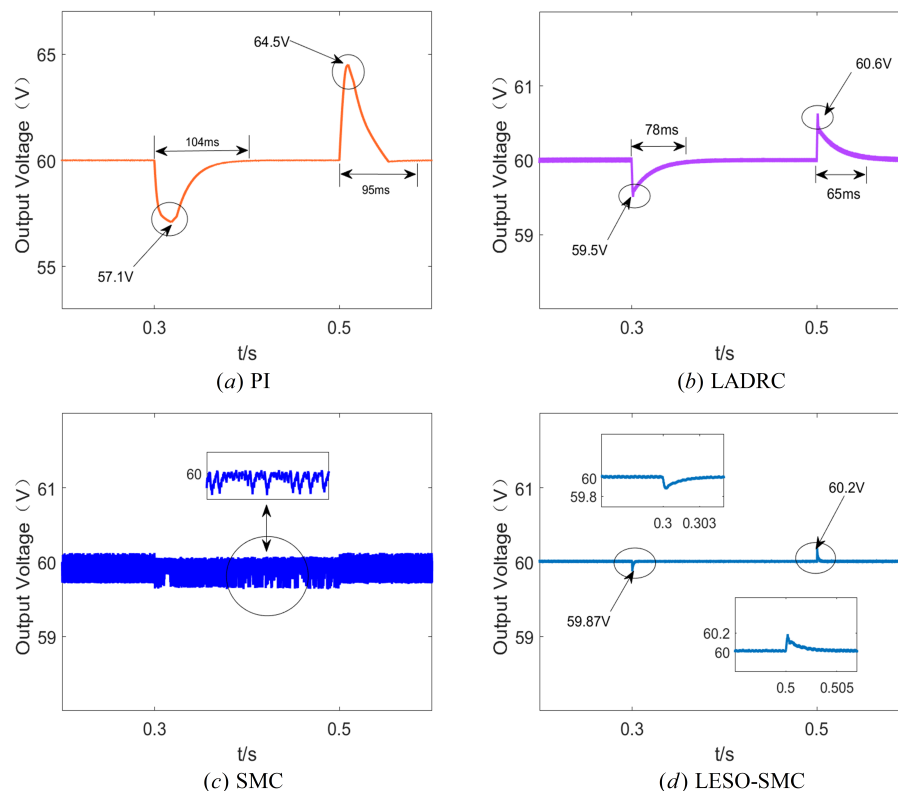


Figure 10. Dynamic waveform of output voltage for four different control strategies under sudden load changes: **(a)** PI, **(b)** LADRC, **(c)** SMC, and **(d)** LESO-SMC.

4.2. Input Voltage Change Experiment

Figures 11 and 12 show the output voltage dynamic response waveforms under the four control methods when the input voltage jumps at 0.4 s. The former depicts the input voltage rising from 110 V to 115 V, and the latter represents the input voltage falling from 110 V to 85 V. In both figures, (a) represents PI control, (b) shows LADRC, (c) denotes SMC, and (d) illustrates the LESO-SMC strategy. Simulation results reveal that the system's output voltage fluctuates with the jump in input voltage. After a certain period, the output voltage will recover to a stable level. As observed in the four subfigures in Figure 11, when the input voltage increases, the output voltage under traditional PI control rises the most, about 0.6 V, and requires the longest adjustment time, around 87 ms. The LADRC strategy experiences a smaller voltage rise, only about 0.1 V, but still requires a long adjustment time of approximately 30 ms. The SMC strategy has virtually no dynamic adjustment process and voltage increase, but from the magnified part of the subfigure Figure 11c, it can be seen that traditional SMC has significant chattering. The control strategy proposed in this paper features an almost negligible voltage rise and virtually no dynamic adjustment time. In the case of a decrease in input voltage, as seen in the four subfigures in Figure 12, the output voltage under PI control drops the most, approximately 0.6 V, with the longest adjustment time of around 92 ms. Under LADRC strategy, the output voltage drop is

smaller, only about 0.1 V, but the adjustment time is still long, around 40 ms. Both SMC and the LESO-SMC strategy proposed in this paper exhibit rapid dynamic responses and stability, but SMC has notable chattering. However, as shown in Figure 12c, there is also notable chattering in the SMC.

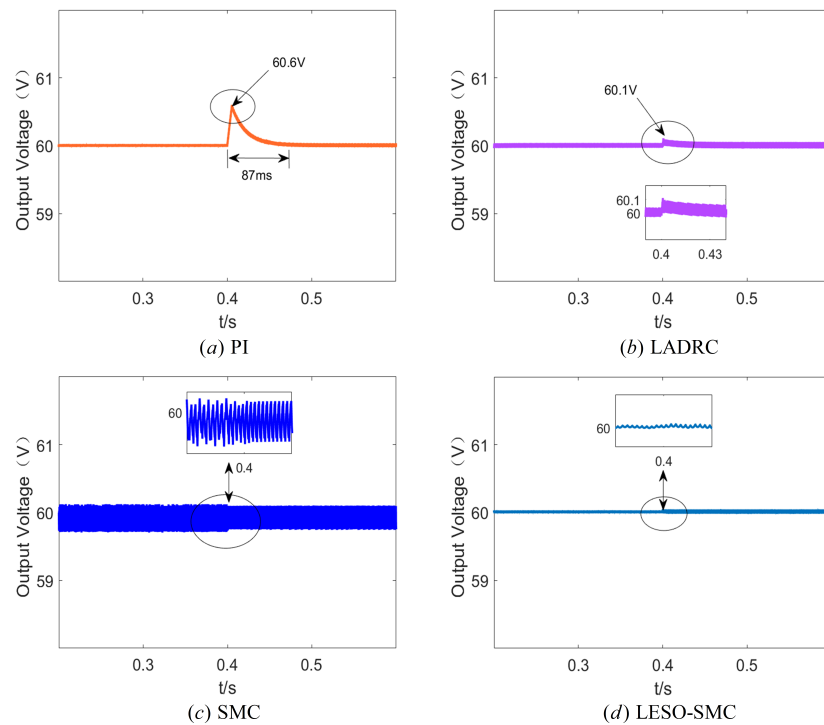


Figure 11. Dynamic waveform of output voltage for four different control strategies when input voltage rises: (a) PI, (b) LADRC, (c) SMC, and (d) LESO-SMC.

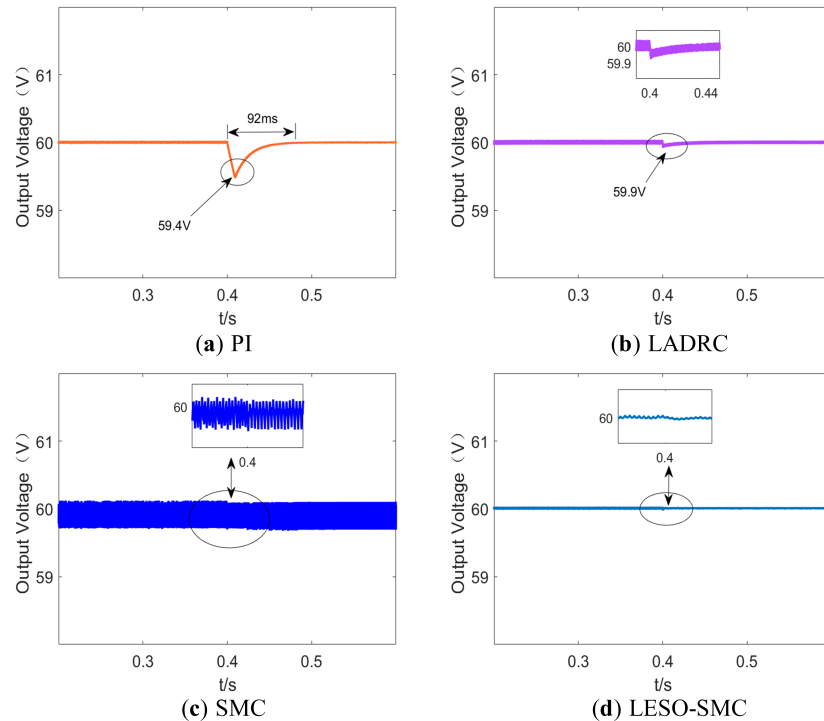


Figure 12. Dynamic waveform of output voltage for four different control strategies when input voltage drops: (a) PI, (b) LADRC, (c) SMC, and (d) LESO-SMC.

4.3. Semi-Physical Experimental Verification

In order to further prove the feasibility and advanced nature of the control strategy mentioned, it is verified on the RT-LAB platform. Figure 13 shows the RT-LAB platform. The lower machine contains multiple real-time simulators that transmit data over the PCIe bus. The selected CPU simulation step is 10 μ s.

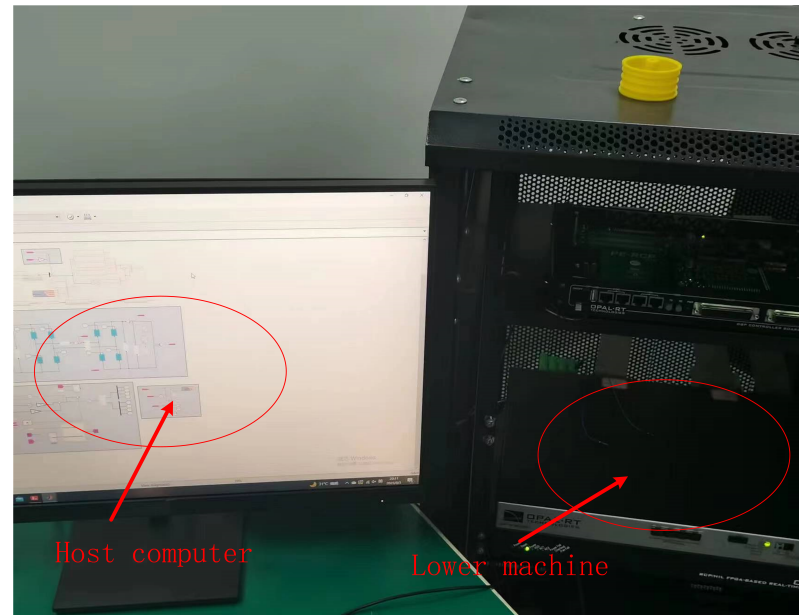


Figure 13. Rt-Lab platform.

Figure 14 shows the load transient waveforms of the four control strategies under the operation of the RT-Lab platform.

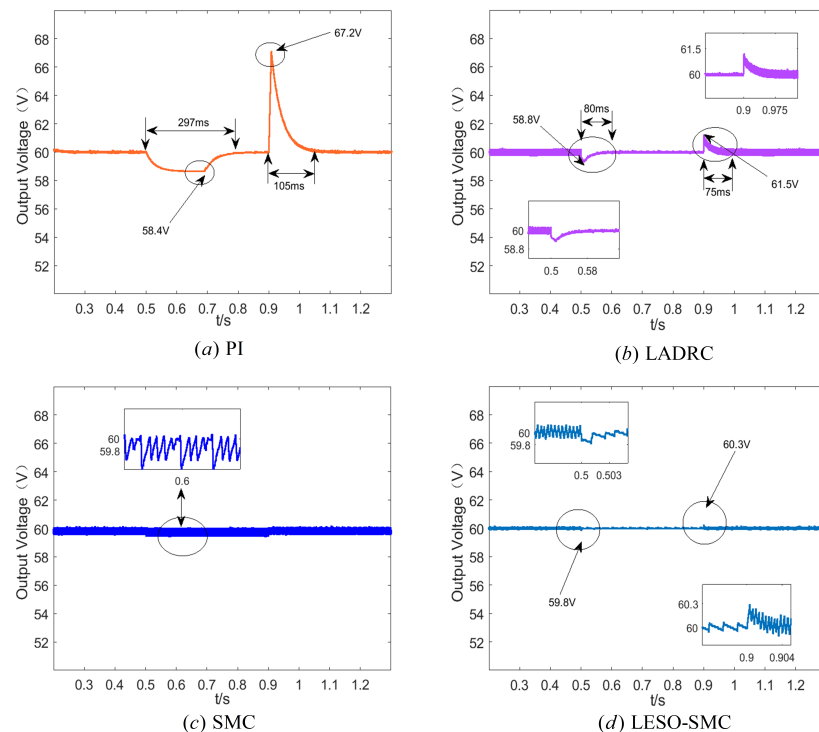


Figure 14. The voltage output waveform diagram when the load changes in the RT-Lab platform: (a) PI, (b) LADRC, (c) SMC, and (d) LESO-SMC.

From Figure 14, it can be observed that under the PI control, when the load changes from full load to half load, the output voltage fluctuates by 2.6 V, and the settling time is 297 ms. When the load is restored, the voltage fluctuation is 7.2 V, and the settling time is 105 ms. Under LADRC strategy, when the load changes from full load to half load, the voltage fluctuates by 1.2 V, and the settling time is 80 ms. When the load is restored, the voltage fluctuation is 1.5 V, and the settling time is 75 ms; Under SMC and LESO-SMC strategies, the response speed is very fast, and the voltage shows minimal fluctuations. However, it is evident that the LESO-SMC strategy does not exhibit noticeable chattering.

Figures 15 and 16 show the output voltage waveforms under the four control strategies on the RT-Lab platform during input voltage rising and falling, respectively.

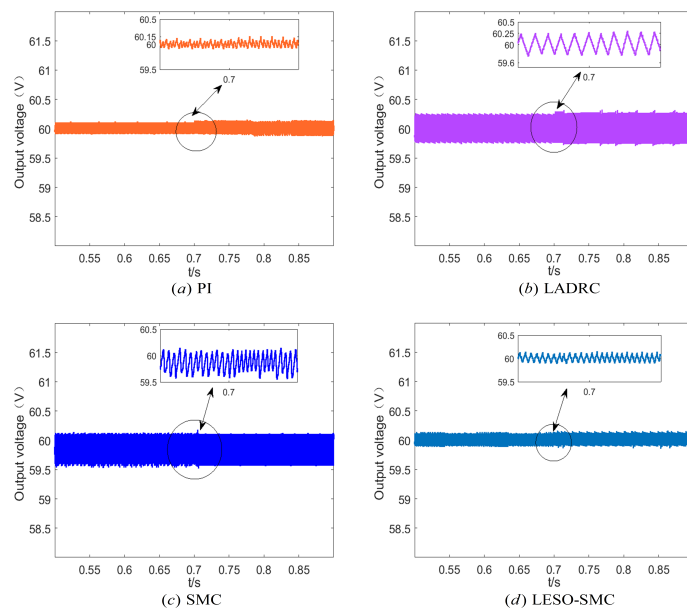


Figure 15. The voltage output waveform diagram when the input voltage rises in the RT-Lab platform: (a) PI, (b) LADRC, (c) SMC, and (d) LESO-SMC.

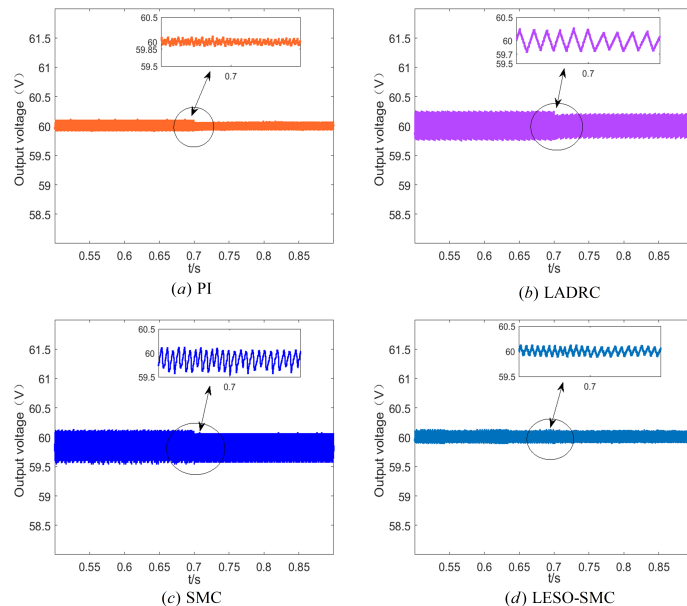


Figure 16. The voltage output waveform diagram when the input voltage drops in the RT-Lab platform: (a) PI, (b) LADRC, (c) SMC, and (d) LESO-SMC.

From Figures 15 and 16, it can be observed that the variation in the input voltage on the RT-Lab platform has a minor impact on the output voltage. Under PI control and LADRC strategy, the voltage slightly increases or decreases. Under SMC and LESO-SMC strategies, the voltage shows almost no fluctuations. However, it is worth noting that, compared to SMC, the LESO-SMC strategy exhibits no significant chattering.

Tables 3 and 4, respectively, compare the performance of the DAB converter under four control strategies, specifically, the voltage fluctuation, adjustment time, and ripple level during sudden load changes and input voltage variations. The comparison results indicate that under the two aforementioned disturbance scenarios, the LESO-SMC strategy proposed in this paper exhibits smaller output voltage fluctuation and superior dynamic response performance compared to PI control and LADRC strategy. Compared to traditional SMC, it does not present obvious chattering issues, making the system more stable. In summary, the LESO-SMC strategy can significantly enhance the system's dynamic performance and anti-interference ability.

Table 3. Performance comparison of four control strategies for load change.

Conditions	Control Methods	Voltages Fluctuation	Adjustment Times	Ripples Level
Form $30\ \Omega$ to $15\ \Omega$	PI	$-2.9\text{ V}/-2.6\text{ V}$	104 ms/297 ms	+/+
	LADRC	$-0.5\text{ V}/-1.2\text{ V}$	78 ms/80 ms	++/+++
	SMC	-/-	-/-	+++/+++
	LESO-SMC	$-0.13\text{ V}/-0.2\text{ V}$	3 ms/3 ms	+/+
Form $15\ \Omega$ to $30\ \Omega$	PI	$+4.5\text{ V}/+7.2\text{ V}$	95 ms/105 ms	+/+
	LADRC	$+0.6\text{ V}/+1.5\text{ V}$	65 ms/75 ms	++/+++
	SMC	-/-	-/-	+++/+++
	LESO-SMC	$+0.2\text{ V}/+0.3\text{ V}$	5 ms/4 ms	+/+

Note: + = Low; ++ = Medium; +++ = High; The slash/behind is the data under the RT-Lab platform.

Table 4. Performance comparison of four control strategies for input voltage changes.

Conditions	Control Methods	Voltages Fluctuation	Adjustment Times	Ripples Level
Form 100 V to 115 V	PI	$+0.6\text{ V}/+0.15\text{ V}$	87 ms/-	++/+
	LADRC	$+0.1\text{ V}/+0.25\text{ V}$	30 ms/-	++/+++
	SMC	-/-	-/-	+++/+++
	LESO-SMC	-/-	-/-	+/+
Form 100 V to 85 V	PI	$-0.4\text{ V}/-0.15\text{ V}$	92 ms/-	++/+
	LADRC	$-0.1\text{ V}/-0.3\text{ V}$	40 ms/-	++/+++
	SMC	-/-	-/-	+++/+++
	LESO-SMC	-/-	-/-	+/+

Note: + = Low; ++ = Medium; +++ = High; The slash/behind is the data under the RT-Lab platform.

5. Conclusions

This paper focuses on the DC-DC converter with good performance required in the distributed electric propulsion system, and selects the DAB converter as the research object. In order to improve the anti-disturbance ability and dynamic performance of the converter, this paper proposes a LESO-SMC strategy as follows:

- (1) Firstly, the principle of SPS control is elaborated in detail, and the reduced order dynamic model is derived. Then, based on this model, the LADRC strategy is designed, and the ability of the LESO to compensate for the system disturbance is used to improve the anti-interference ability and dynamic performance of the converter.
- (2) In order to further improve the performance of the converter, the LESO is combined with SMC, and the nonlinear error feedback law constructed by the observer's value and the switching function can better adapt to the nonlinear characteristics of the converter, which is no serious chattering phenomenon.

- (3) Finally, the strategy is verified on the Matlab/Simulink and RT-Lab platform. The theoretical and experimental results show that the LESO-SMC strategy proposed in this paper has stronger robustness and better dynamic performance under the conditions of load mutation and input voltage change and can achieve a stable tracking of the output reference voltage.

Author Contributions: Thesis conception, M.Y. and P.L.; methodology M.Y. and P.L.; Data analysis and visualization, M.Y. and P.L.; Preparation of the original manuscript, P.L.; Written comments and editing, M.Y.; project administration, M.Y. All authors have read and agreed to the published version of the manuscript.

Funding: This research was partially funded by the National Natural Science Foundation of China (Grant no. 2020jj6061), Hunan Provincial Natural Science Foundation Regional Joint Fund (Grant no. 2023jj50052), the Science Furthermore Technology Innovation Program of Hunan Province (Grant no. 2021GK2010), and Project 62273142 supported by National Natural Science Foundation of China.

Data Availability Statement: The data presented in this study are available in the text.

Conflicts of Interest: The authors declare no conflict of interest.

References

1. Kong, X.; Zhang, Z.; Lu, J.; Li, J.; Yu, L. Review of electric power system of distributed electric propulsion aircraft. *Acta Aeronaut. Astronaut. Sin.* **2018**, *39*, 46–62. [[CrossRef](#)]
2. Buticchi, G.; Costa, L.; Liserre, M. Improving system efficiency for the more electric aircraft: A look at DC/DC converters for the avionic onboard dc microgrid. *IEEE Ind. Electron. Mag.* **2017**, *11*, 26–36. [[CrossRef](#)]
3. Jiang, J.; Zhang, T.; Chen, D. Analysis, design, and implementation of a differential power processing DMPPT with multiple buck-boost choppers for photovoltaic module. *IEEE Trans. Power Electron.* **2021**, *36*, 10214–10223. [[CrossRef](#)]
4. Hou, N.; Song, W.; Li, Y.; Zhu, Y.; Zhu, Y. A comprehensive optimization control of dual-active-bridge DC–DC converters based on unified-phase-shift and power-balancing scheme. *IEEE Trans. Power Electron.* **2018**, *34*, 826–839. [[CrossRef](#)]
5. Bai, H.; Mi, C.; Wang, C.; Gargies, S. The dynamic model and hybrid phase-shift control of a dual-active-bridge converter. In Proceedings of the 2008 34th Annual Conference of IEEE Industrial Electronics, Orlando, FL, USA, 10–13 November 2008; pp. 2840–2845. [[CrossRef](#)]
6. Bai, H.; Nie, Z.; Mi, C.C. Experimental comparison of traditional phase-shift, dual-phase-shift, and model-based control of isolated bidirectional DC–DC converters. *IEEE Trans. Power Electron.* **2009**, *25*, 1444–1449. [[CrossRef](#)]
7. Qin, H.; Kimball, J.W. Generalized average modeling of dual active bridge DC–DC converter. *IEEE Trans. Power Electron.* **2011**, *27*, 2078–2084. [[CrossRef](#)]
8. Shi, L.; Lei, W.; Li, Z.; Huang, J.; Cui, Y.; Wang, Y. Bilinear discrete-time modeling and stability analysis of the digitally controlled dual active bridge converter. *IEEE Trans. Power Electron.* **2016**, *32*, 8787–8799. [[CrossRef](#)]
9. Hou, N.; Song, W.; Wu, M. Direct power control scheme of full-bridge isolated DC/DC converters. *Dianli Xitong Zidonghua/Autom. Electr. Power Syst.* **2016**, *40*, 204–209. [[CrossRef](#)]
10. Song, W.; Hou, N.; Wu, M. Virtual direct power control scheme of dual active bridge DC–DC converters for fast dynamic response. *IEEE Trans. Power Electron.* **2017**, *33*, 1750–1759. [[CrossRef](#)]
11. Hou, N.; Song, W.; Mingyi, W. A load current feedforward control scheme of dual active bridge DC/DC converters. *Proc. CSEE* **2016**, *36*, 2478–2485. [[CrossRef](#)]
12. Tarisciotti, L.; Chen, L.; Shuai, S.; Dragicevic, T. Large signal stability analysis of DAB converter using moving discretized control set–model predictive control. In Proceedings of the 2020 IEEE Energy Conversion Congress and Exposition (ECCE), Detroit, MI, USA, 11–15 October 2020; pp. 5922–5929. [[CrossRef](#)]
13. Chen, L.; Gao, F.; Shen, K.; Wang, Z.; Tarisciotti, L.; Wheeler, P.; Dragičević, T. Predictive control based DC microgrid stabilization with the dual active bridge converter. *IEEE Trans. Ind. Electron.* **2020**, *67*, 8944–8956. [[CrossRef](#)]
14. An, F.; Song, W.; Yang, K. Model predictive control and power balance scheme of dual-active-bridge DC–DC converters in power electronic transformer. *Proc. CSEE* **2018**, *38*, 3921–3929. [[CrossRef](#)]
15. Zeng, Y.; Maswood, A.I.; Pou, J.; Zhang, X.; Li, Z.; Sun, C.; Mukherjee, S.; Gupta, A.K.; Dong, J. Active disturbance rejection control using artificial neural network for dual-active-bridge-based energy storage system. *IEEE J. Emerg. Sel. Top. Power Electron.* **2021**, *11*, 301–311. [[CrossRef](#)]
16. Nie, J.; Zhao, Z.; Yuan, L.; Duan, R.; Shi, B.; Jin, L. An energy balance active disturbance rejection control for improving converter stability while maintaining fast dynamic performance. *IEEE Trans. Power Electron.* **2020**, *35*, 11304–11309. [[CrossRef](#)]
17. Jeung, Y.C.; Lee, D.C. Voltage and current regulations of bidirectional isolated dual-active-bridge DC–DC converters based on a double-integral sliding mode control. *IEEE Trans. Power Electron.* **2018**, *34*, 6937–6946. [[CrossRef](#)]

18. Li, K.; Yang, Y.; Tan, S.C.; Hui, R.S.Y. Sliding-mode-based direct power control of dual-active-bridge DC-DC converters. In Proceedings of the 2019 IEEE Applied Power Electronics Conference and Exposition (APEC), Anaheim, CA, USA, 17–21 March 2019; pp. 188–192. [[CrossRef](#)]
19. Chen, W.H.; Yang, J.; Guo, L.; Li, S. Disturbance-observer-based control and related methods—An overview. *IEEE Trans. Ind. Electron.* **2015**, *63*, 1083–1095. [[CrossRef](#)]
20. Xiong, F.; Wu, J.; Liu, Z.; Hao, L. Current sensorless control for dual active bridge DC-DC converter with estimated load-current feedforward. *IEEE Trans. Power Electron.* **2017**, *33*, 3552–3566. [[CrossRef](#)]
21. Meng, X.; Jia, Y.; Xu, Q.; Ren, C.; Han, X.; Wang, P. A Novel Intelligent Nonlinear Controller for Dual Active Bridge Converter With Constant Power Loads. *IEEE Trans. Ind. Electron.* **2022**, *70*, 2887–2896. [[CrossRef](#)]
22. Wu, Y.; Mahmud, M.H.; Zhao, Y.; Mantooth, H.A. Uncertainty and disturbance estimator-based robust tracking control for dual-active-bridge converters. *IEEE Trans. Transp. Electrif.* **2020**, *6*, 1791–1800. [[CrossRef](#)]
23. Shao, S.; Chen, L.; Shan, Z.; Gao, F.; Chen, H.; Sha, D.; Dragičević, T. Modeling and advanced control of dual-active-bridge DC-DC converters: A review. *IEEE Trans. Power Electron.* **2021**, *37*, 1524–1547. [[CrossRef](#)]
24. Abdul-Adheem, W.R.; Ibraheem, I.K. Improved sliding mode nonlinear extended state observer based active disturbance rejection control for uncertain systems with unknown total disturbance. *Int. J. Adv. Comput. Sci. Appl.* **2016**, *7*, 80–93. [[CrossRef](#)]
25. Ma, Y.; Wen, H.; Zhou, X.; Yin, J. Modeling and Control Strategy Simulation of Dual Active Bridge DC-DC Converter. In Proceedings of the 2021 IEEE International Conference on Mechatronics and Automation (ICMA), Takamatsu, Japan, 8–11 August 2021; pp. 431–435. [[CrossRef](#)]
26. Gao, Z. Scaling and bandwidth-parameterization based controller tuning. In Proceedings of the 2003 American Control Conference, Denver, CO, USA, 4–6 June 2003; pp. 4989–4996. [[CrossRef](#)]
27. Tan, S.C.; Lai, Y.; Chi, K.T. Indirect sliding mode control of power converters via double integral sliding surface. *IEEE Trans. Power Electron.* **2008**, *23*, 600–611. [[CrossRef](#)]
28. Tiwary, N.; Panda, A.K.; Lenka, R.K.; Narendra, A. Super twisting sliding mode control of dual active bridge DC-DC converter. In Proceedings of the 2020 IEEE International Conference on Power Electronics, Drives and Energy Systems (PEDES), Jaipur, India, 16–19 December 2020; pp. 1–5. [[CrossRef](#)]
29. Tiwary, N.; Panda, A.K.; Narendra, A.; Lenka, R.K. A Robust Voltage Control of DAB Converter With Super-Twisting Sliding Mode Approach. *IEEE J. Emerg. Sel. Top. Ind. Electron.* **2022**, *4*, 288–298. [[CrossRef](#)]

Disclaimer/Publisher’s Note: The statements, opinions and data contained in all publications are solely those of the individual author(s) and contributor(s) and not of MDPI and/or the editor(s). MDPI and/or the editor(s) disclaim responsibility for any injury to people or property resulting from any ideas, methods, instructions or products referred to in the content.